The cool-flame chemistry of tetrahydropyran: Insights into oxygenated heterocyclic ring dynamics

Jiabiao Zou, Caroline Smith Lewin, Weiye Chen, Cheng Xie, Zhandong Wang, Jérémy Bourgalais, Olivier Herbinet, Frédérique Battin-Leclerc, Aamir Farooq

The cool-flame chemistry of tetrahydropyran: Insights into oxygenated heterocyclic ring dynamics

Jiabiao Zou[1,*], Caroline Smith Lewin[2], Weiye Chen[3], Cheng Xie[3], Zhandong Wang[3], Jérémy Bourgalais[2,*], Olivier Herbinet[2], Frédérique Battin-Leclerc[2], Aamir Farooq[1,*]

1. Physical Sciences and Engineering, King Abdullah University of Science and Technology, Thuwal 23955-6900, Kingdom of Saudi Arabia

2. LRGP, Université de Lorraine, CNRS, F-54000 Nancy, France

3. National Synchrotron Radiation Laboratory, University of Science and Technology of China, Hefei, Anhui 230029, P. R. China

Abstract

The oxidation of tetrahydropyran (THP) was investigated in two atmospheric jet-stirred reactors over temperatures of 450-900 K and equivalence ratios of 0.25-1.0. Utilizing synchrotron vacuum ultraviolet photoionization mass spectrometry (SVUV-PIMS) and gas chromatography (GC) methods, we qualitatively and quantitatively analyzed dozens of intermediates, including C_1-C_4 carbonyl compounds, conjugated olefins, cyclic ethers, and reactive hydroperoxides. This comprehensive analysis provided insights into the cool flame chemistry of THP. For the first time, we observed remarkable low-temperature oxidation reactivity and negative temperature coefficient (NTC) behavior during THP oxidation. Quantum chemistry calculations, including adiabatic ionization energy and appearance potential energy calculations, were performed to identify reaction products. Additionally, energy barrier analysis of key reactions allowed an exploration of the effects of the ether group in intramolecular H-transfer. Our proposed model introduces a conformational-dependent THP oxidation sub-mechanism, enhancing predictability and highlighting the intricate low-T chemistry of THP. Rigorous validation against current and literature experimental data across diverse conditions demonstrated high accuracy. We found that the ether group in the heterocycle ring can enhance C-H bond energy at its *meta*-sites and weaken C-H bond energy at its *ortho*-sites of key radicals (e.g., ROO, OOQOOH). In the low-T region, β-tetrahydropyranyl preferentially undergoes chain inhibition, while chain-branching reactions become more favorable for reaction sequences originating from α- and γ-tetrahydropyranyl. With increasing temperature, the ring-opening of α- and β-tetrahydropyranyl radicals becomes more competitive, leading to a pronounced NTC behavior in THP oxidation.

Keywords: Tetrahydropyran; Biofuel; Low-temperature oxidation; Jet-stirred reactor; Kinetic model.

[*] Corresponding author. Email: jiabiao.zou@kaust.edu.sa; Jeremy.bourgalais@cnrs.fr; aamir.farooq@kaust.edu.sa.

Information for Colloquium Chairs, Editors, and Reviewers

Novelty and Significance Statement

This study makes a significant contribution to advancing renewable transportation energy by addressing the underexplored low-temperature (low-T) oxidation chemistry of tetrahydropyran (THP), a promising lignocellulosic-derived biofuel. While THP has been extensively studied at high temperatures, low-T oxidation remains a crucial knowledge gap. This work utilizes advanced techniques, including synchrotron vacuum ultraviolet photoionization mass spectrometry (SVUV-PIMS) and gas chromatography (GC), to analyze intermediates qualitatively and quantitatively in THP cool flame chemistry. The investigation explores the influence of the ether group on chain-inhibition and chain-branching steps, employing energy barrier calculations and comprehensive kinetic modeling. This research significantly contributes to a deeper understanding of the low-T oxidation kinetics of THP, paving the way for informed advancements in renewable transportation energy.

1) Author Contributions

- JZ: conception, designed research, performed experiments, analyzed data, kinetic modeling, wrote and revise manuscript.
- CSL: performed experiments, analyzed data.
- WC: performed experiments.
- CX: performed experiments.
- ZW: supervision, funding acquisition, methodology, review manuscript
- JB: methodology, supervision, analyzed data, manuscript revision.
- OH: performed experiments, methodology, review manuscript.
- FBL: supervision, funding acquisition, manuscript revision
- AF: supervision, funding acquisition, methodology, manuscript revision

2) Authors' Preference and Justification for Mode of Presentation at the Symposium

The authors prefer **OPP** presentation at the Symposium, for the following reasons:

- This research marks the first-ever exploration of comprehensive speciation measurements and kinetic modeling of the low-T oxidation of tetrahydropyran (THP) in the jet-stirred reactor.
- This research addresses the first to third oxygen addition schemes for a representative lignocellulosic-derived biofuel, THP, with the observation of dozens of intermediates.
- We introduce a novel conformational-dependent reaction scheme for oxygenated cyclic molecules, effectively addressing the gap between molecular structure and oxidation behavior.
- The unique combined research method for the relatively unexplored THP molecule was conducted, addressing a crucial knowledge gap in carbon-neutral fuel development. Such illustrations and analysis will lead to an intriguing room-level discussion.

1. Introduction

As we strive for a carbon-neutral future, a fundamental imperative lies in minimizing the carbon footprint associated with the transportation sector. A strategic approach towards this goal involves the substitution of fossil fuels with renewable fuels. Among alternative options, lignocellulosic-derived biofuels have attracted considerable attention for their potential as renewable sources of transportation energy. The production of these biofuels entails the intricate deconstruction of lignocellulosic biomass—a complex matrix primarily composed of cellulose, hemicellulose, and lignin, housing a diverse array of substituted five- and six-membered cyclic components [1]. Among lignocellulosic-derived biofuels, tetrahydropyran (THP), the simplest lignocellulose-derived biofuel, has emerged as a promising candidate for sustainable energy. Its structural similarities with glucose and fructose, coupled with its potential to yield reduced-carbon-intensity transportation fuels, underscore its viability for contributing to a sustainable energy landscape [2, 3]. Furthermore, THP can be a suitable candidate for exploring the chemistry of the cyclic lignocellulosic biofuel family, finding applications to cyclic ether-based biofuels and fuel additives [2, 3].

A substantial body of experimental research has delved into the high-temperature (high-T) pyrolysis and oxidation of THP, encompassing investigations into ignition delay times (IDT), laminar burning velocities, species profiles in flow reactor pyrolysis and jet-stirred reactor (JSR) oxidation, as well as flame structure in low-pressure laminar premixed flames [4-6]. These studies span temperatures of 800-1700 K and pressures of 1.7-10 bar. A recent review by Rotavera and Taatjes [2] and Tran et al. [3] comprehensively outlined the details of THP combustion and pyrolysis and noted that "*The unclear chemistry involving the ether-group in the heterocycle ring and its corresponding ring-opening reactions may inhibit ketohydroperoxide formation and lead to diminished NTC behavior in THP*".

For kinetic modeling, Dagaut et al. [5] developed the first chemical kinetics mechanism with lumped species to interpret their measured data in JSR and shock tube. Subsequently, Labbe et al.[6] expanded the THP high-T sub-mechanism by incorporating the calculated rates of fuel radicals ring-opening reactions to understand the measured speciation in a premixed flame. Tran et al. [4] further explored the pyrolysis chemistry and high-T oxidation chemistry with an extended THP high-T subset, incorporating one pericyclic rearrangement reaction and three ring opening reactions.

Despite the extensive examination of high-T chemistry of THP, its low-temperature (low-T) oxidation chemistry has received limited attention. Only four prior works have undertaken preliminary experimental exploration of THP low-T oxidation chemistry during chlorine-initiated oxidation processes, while no effective experimental data was reported for kinetic modeling. Rotavera et al. [7], Davis et al. [8], Chen et al. [9], and Telfah et al. [10] conducted studies for chlorine-initiated THP oxidation at low temperatures, employing various techniques such as multiplexed photoionization mass spectrometry (MPIMS) [7, 8], time-resolved infrared absorption method [9], cavity ring-down spectroscopy (CRDS) [10]. Rotavera et al. [7] revealed that the ether group facilitates chain-inhibiting via concerted HO_2-elimination of tetrahydropyranyl peroxy radicals at lower temperatures, whereas the ring-opening reactions via C-O bonds β-scission of tetrahydropyranyl become dominant at higher temperatures. This conclusion was further confirmed by Chen et al.[9] by monitoring OH and HO_2 time histories at 500-750 K and 20 Torr. Moreover, Telfah et al. [10] attributed the absence of α-THPOO in their CRDS spectra to the competition of ring-opening reaction of α-tetrahydropyranyl radical. Davis et al. [8] observed the photoionization spectra of ketohydroperoxides (KHPs) and demonstrated the existence of O_2+QOOH pathways in THP low-T oxidation. They confirmed the depletion of QOOH by observing 3-butenal, vinyl formate and pentanedial (glutaraldehyde). Davis et al.[8] pointed out that the β-scission of R and QOOH radicals are more pronounced in THP compared to cyclohexane, diminishing KHPs formation in THP.

Given the scarcity of studies on low-T oxidation chemistry of THP, there exists a crucial knowledge gap that necessitates comprehensive experimental measurements and kinetic modeling of this important heterocycle ring molecule. This work endeavors to address this gap by qualitatively and quantitatively analyzing the speciation data collected in two atmospheric JSRs, employing single-photon synchrotron vacuum ultraviolet photoionization mass spectrometry (SVUV-PIMS) and gas chromatography (GC), at low to intermediate temperatures. The investigation seeks to elucidate the influence of the ether group on chain-inhibition and chain-branching steps involving carbon-centered radicals (R, QOOH, and $P(OOH)_2$), employing energy barrier calculations as well as comprehensive kinetic modeling and modeling analysis. Through these efforts, this study contributes to a deeper understanding of the intricate kinetics governing the low-T oxidation chemistry of THP, facilitating informed advancements in the realm of renewable transportation energy.

2. Methodologies

2.1 Jet-stirred reactor & SVUV-PIMS (NSRL-JSR)

Oxidation experiments of THP in a JSR coupled to SVUV-PIMS were performed at BL09U beamline (NSRL, China). The beamlines and apparatus have been described in detail elsewhere [11]. Generally, SVUV-PIMS covers the ionization photon energies of all oxidation intermediates and provides excellent mass resolution (5000 at m/z = 100) and detection limit (0.1 ppm). The JSR has a volume of 78 cm^3 with a quartz sampling nozzle of ~80 μm orifice on the tip. Reacting gases were sampled from the JSR due to the low background pressure in the vacuum chamber. THP (>99.5% purity) was injected into an electrically heated vaporizer through a syringe pump. Gas flow rates of argon (99.9999% purity) and oxygen (99.9999% purity) were regulated with mass flow controllers. All gases were piped through a preheating section before being injected into the JSR to ensure temperature homogeneity in the reactor. JSR temperature was controlled by a

custom-made tube furnace. The residence time in the preheating section is negligible compared to that in the JSR. Reaction temperature is monitored using a K-type thermocouple (±2 K) located at the center of the JSR. Initial mole fraction of fuel was kept at 0.5% (molar) at an equivalence ratio of 0.25. Total inlet flow rate was varied to maintain a residence time of 4 s for various operating temperatures. Identification and mole fraction evaluation of the measured species were performed according to the method described previously [12]. Mole fraction uncertainties in our experiments were ±10% for reactants (THP, O_2), ±20% for major products (CO, CO_2, etc.) evaluated from cold gas calibration, ±30% for species with known photoionization cross sections (PICSs), and a factor of 2 for species with estimated PICSs. Species identification results and PICS sources of detected species are summarized in Tables S1, S2 and Figs. S1-S5 in *Supplementary Materials* (*SM*).

2.2 *Jet-stirred reactor & GC-MS (LRGP-JSR)*

A similar JSR was employed to measure stable species using three GCs at LRGP (Nancy, France). This apparatus has been comprehensively described in a recent paper [13]. The first GC fitted with a Q-Bond capillary column and a flame ionization detector (FID) preceded by a methanizer, is adopted for the quantification of C_1-C_5 compounds (e.g., CH_4, CO, CO_2, ethylene, propene, etc.). The methanizer (nickel catalyst for hydrogenation) allows the detection of species like CO and CH_3CHO with a better sensitivity. The second GC, equipped with a HP-5 capillary column and an FID, is adopted for quantification of heavier species (containing more than 5 carbons). A third GC, equipped with both HP-5 and Q-Bond capillary columns and coupled to a mass spectrometer (quadrupole) with electron ionization at 70 eV, allows the identification of the cyclic ethers, conjugated olefins and carbonyl species. Initial mole fraction of fuel was kept at 0.5% (molar) at three equivalence ratios of 0.25, 0.5, 1.0. The residence time was kept at 4 s for various operating temperatures. Calibrations are performed by injecting standards when available, with uncertainties in mole fractions evaluations to be around ±5%. For other species calibrated using the effective carbon number method have mole fraction uncertainties of ±10%. Satisfactory concordance was achieved for the data from NSRL- and LRGP-JSR, as illustrated in *Section 4.2*.

2.3 *Theoretical calculations*

Adiabatic ionization energies (IEs) and appearance potential energies (APEs) of key species were calculated to identify intermediates from SVUV-PIMS experiments. Energy barriers of ROO and OOγQOOH 1,5-H transfer pathways were calculated to explore the conformational effects of heterocycle ring. The lowest energy conformation structures were obtained from relaxed scans around each rotor in 10° using B3LYP/6-311++G(d,p) [14]. Structures and single-point energies of intermediates were calculated at CBS-QB3 level using Gaussian 09 [15]. Uncertainty of calculated energy values is expected to be less than 1.5 kcal/mol. The uncertainties of calculated IEs for large hydroperoxides and highly oxygenated molecules (HOMs) are estimated to be ±0.15 eV due to the larger number of conformers and isomers of these molecules [16-18].

3. Kinetic modeling

The current mechanism was constructed based on the comprehensive cyclohexane model of Zou et al. [16]. AramcoMech 2.0 [19] serves as the foundational mechanism, with the incorporation of conformational-dependent low-T reaction classes proposed by Zou et al. [16, 17] for cycloalkanes, and specifically tailored here to describe THP oxidation sub-mechanism. The high-T and low-T reaction classes utilized in the model, along with the sources of their rate constants, are elucidated in Table S4, with the chemical structures of species illustrated in Table S5 (*SM*). Thermodynamic data of newly identified species in this work were estimated using the group-additivity method [20].

The subset addressing the high-T combustion and pyrolysis of THP stems from the work of Tran et al.[4]. In the current mechanism, by analogies to tetrahydrofuran [21], two pathways were added to better describe the fuel consumption: (1) the ring-opening of the heterocycle ring through C-O and C-C bond fissions to yield diradical species, which further decompose to aldehydes and olefins; (2) pericyclic hydrogen elimination resulting in cyclic diradical formation.

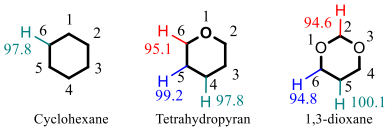

Fig. 1. Bond dissociation energies (BDEs) of C-H bonds in cyclohexane [22], tetrahydropyran and 1,3-dioxane [23].

The consumption of THP predominantly occurs through H-abstraction reactions involving OH and HO_2. Experimental measurements by Moriarty et al. [24] and calculations by Saheb and Bahador [25] provided crucial insights into the rates of H-abstraction reactions by OH of molecules with oxygenated heterocycle ring. Figure 1 illustrates the similarity in C-H bond dissociation energies (BDE) between specific sites in THP and analogous sites in cyclohexane and 1,3-dioxane. This resemblance allows the adoption of calculated rates for certain sites, ensuring the accuracy of the kinetic model. Concurrently, the rates of THP+OH reactions at sites 2 and 6 were extrapolated from analogous carbon sites of 1,4-dioxane, utilizing both theoretical calculations spanning the temperature range of 200-1000 K [25] and experimental findings within the range of 263-372 K [24]. THP+OH rates at sites 3 and 5 were determined by accounting for their analogical characteristics to the site 5 of 1,3-dioxane. More details on this are given in Section S2 (*SM*). For THP+HO_2, the rates of site 2 and 3 were referred to 1,3-dioxane+HO_2 [26] with the corrected activation energy based on the BDE difference in Fig.1, while the rate from site 4 was refer to cyclohexane+HO_2 [27].

The fuel radicals can either undergo β-scission to break the heterocyclic ring or undergo barrierless oxygen addition forming peroxy radicals (THPROO2, THPROO3, and THPROO4). Those ROO radicals include two conformers, RaOO with axial-peroxy and

ReOO with equatorial-peroxy.; "a" and "e" denotes the functional group at axial and equatorial position, respectively. The numbering of species in the current work denotes the sites in the heterocycle ring, as illustrated in Fig.1. Based on the conclusions of Zou et al. [16] for cyclohexane, the rapid inversion-topomerization processes of the six-membered ring facilitate fast equilibrium between axial and equatorial conformers. This can greatly counterbalance the influence of initial positions of the side-chain groups in ROO and QOOH in cyclohexane oxidation. The heterocycle ring in THP is very similar to cyclohexane ring in cyclohexane, thus, only RaOO is considered in the present model. ROO undergoes intramolecular H transfer to form QOOHs， i.e., αQOOH, βQOOH, γQOOH, and δQOOH, via four-membered transition state (4mTS), 5mTS, 6mTS and 7mTS, respectively. Compared with cyclohexane, the oxygen atom in THP block partial of βQOOH, γQOOH, and δQOOH formation from THPROO2, THPROO3 and THPROO4, respectively. Formation of HO_2 from the chemical activation channel of R+O_2, the concerted elimination of ROO and unimolecular decomposition of βQOOH were adopted in present model.

To our knowledge, theoretically calculated rates of THP low-T oxidation are not available in the literature. In the present model, the entrance channel of R+O_2, the intramolecular H-transfer, and the concerted elimination of ROO, the cyclization of QOOH, and the decomposition of βQOOH are estimated based on similar reactions in cyclohexane [16] and 1,3-dioxane [28]. Following factors are considered to determine the rate of specific reactions, including (i) the size of the formed transition sate, i.e., 5mTS, 6mTS, and 7mTS; (ii) the composition of the formed transition sates, particularly considering if O from the heterocycle ring is involved or not; (iii) the type of carbon site with peroxy or hydroperoxy group; (iv) the type of abstracted hydrogen, i.e., *ortho-*, *meta-*, or *para-* site of oxygen. Detailed information is shown in Table S4 (*SM*).

Unimolecular decomposition pathways of fuel radicals and QOOH radicals, particularly via β-scission of C-O at the α-site, play a vital role in THP low-T oxidation in contrast to cyclohexane [7-10], emphasizing the unique behavior of THP. Tran et al. [4] calculated the rates of concerted C-C and C-O β-scission for fuel radicals, which are adopted in the current model for fuel radicals and QOOH unimolecular decomposition reactions via C-C and C-O β-scission. Specifically, the decomposition product (PC4H8CHO-4) from γQOOH C-O β-scission is considered to undergo oxygen addition and intramolecular H-transfer. The former one can leads to chain-branching via the conventional KHP pathway, while the later one results in chain-inhibition.

The conformational effects of the heterocycle ring further contribute to the complexity of the kinetic model. The intricacies of these reactions are carefully considered, drawing parallels to similar reactions in cyclohexane. Further details concerning conformational analysis involving the first and second oxygen addition are provided in Section S2.1 (*SM*). Generally, the prevailing role of γQOOH formed from the first oxygen addition is highlighted in the second oxygen addition, with specific conformers considered for simplicity. The kinetic model addresses the steric hindrance effects of additional hydroperoxyl groups in the intramolecular H-transfer of OOγQOOH. Similar to cyclohexane, the entrance channels of γQOOH+O_2 are treated to form 55% *trans*-OOγQOOH and 45% *cis*-OOγQOOH conformers and undergo subsequent intramolecular H-transfer leading to γKHPs and γP(OOH)$_2$, respectively, as shown in Fig. S6 (*SM*). γP(OOH)$_2$ further decomposes into alkenyl-hydroperoxide (AnHP) and OH through two channels, (a) unimolecular decomposition to AnHP+OH; (b) cyclization to a 4-membered cyclic ether hydroperoxide (4mCEHP), which then rapidly isomerizes to AnHP.

The rate constants of the entrance channel of QOOH+O_2 are referred to similar reactions in the first oxygen addition with the pre-exponential factor divided by two to consider the steric hindrance effects of the additional hydroperoxyl group. Specifically, the rate of *trans*-OOγQOOH↔γKHP+OH is adopted from the similar reaction in the first oxygen addition directly. As shown in Fig. 2, the energy barrier of conventional isomerization of OOγQOOH is only 0.5 kcal/mol lower than the alternative isomerization pathway, which is significantly different from the observed discrepancy of similar pathways in cyclohexane [18] and propane [29]. Other reactions involving OOQOOH and P(OOH)$_2$ decomposition are referred to the similar reaction of ROO and QOOH in the first oxygen addition.

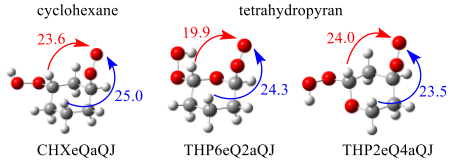

Fig. 2. Calculated energy barrier of 1,5-H shift in OOγQOOH in cyclohexane [18] and tetrahydropyran.

4. Results and discussion

4.1 Identification of reaction intermediates

In this work, dozens of intermediates were observed, particularly a variety of hydroperoxides and their decomposition products, which were detected and identified using SVUV-PIMS. Conjugated olefins and cyclic ethers were further separated using GC. Figure S1 (*SM*) illustrates a mass spectrum over m/z = 30-170. Subsequent analysis utilized photoionization efficiency (PIE) spectra, illustrated in Fig.3 and Figs. S2-S4 (*SM*), for representative hydroperoxides and their decomposition products. Given the complexity of fuel-specific oxygenated intermediates and the abundance of isomers and conformers, the identification of all candidate isomers from a single mass peak is not feasible. Consequently, IE calculations were selectively conducted for representative structures, guided by observed ionization thresholds, the chemical nature and thermal stability of potential candidates, and the simulated mole fractions. Tables S1 and S2 in *SM* enumerate the observed species and their corresponding calculated IEs.

The agreement between observed ionization thresholds on PIE spectra and the lower boundaries of calculated IEs validates the existence of key structures.

Notably, in Fig. 3, structures corresponding to m/z=116, 118, and 132 align with OFHP ($C_5H_8O_3$), ROOH ($C_5H_{10}O_3$), and KHP/AnHP/CEHP ($C_5H_8O_4$), respectively, affirming the presence of a conventional two-stage oxygen addition scheme. Figures S3(e) and S3(f) further support this correlation, linking the calculated IEs of olefinic ketone ($C_5H_6O_2$) and diketone ($C_5H_6O_3$) isomers to experimental onsets of PIE spectra for m/z=98 and m/z=114. The observed ionization thresholds for m/z=132 align with the calculated IEs of THP15DK3Q ( , 9.21 eV) and THP3K5Q ( , 9.11[a]/9.17[e] eV), corroborating the involvement of the formation channels of γKHP and AnHP mediated with *trans*-OOγQOOH and *cis*-OOγQOOH, respectively. However, the reaction sequence involving in THP3K5Q formation are identified as minor channel, see details from *Section 4.2*. Figure S7 (*SM*) elucidates multiple dissociation pathways for γKHP generating various products such as CO_2, C_2H_4, CH_2O, CH_2CO, while that formed from AnHP produces 3-butenal, malonaldehyde (), vinyl formate (), formic anhydride (), formic acid. Those products were detected in the present work, as shown in Fig. S3 and Table S1 in *SM*. Experimental confirmation of 3-butenal and vinyl formate formation aligns with the findings of Davis et al. [8], underlining the contribution of ring-opening reactions involving R, QOOH, and $P(OOH)_2$ to 3-butenal and vinyl formate production. It is worth noting that the first and second ionization thresholds on the PIE spectra of m/z=114 ($C_5H_6O_3$), near 9.20 and 9.80 eV locate close to the calculated IEs of acyclic carbonyl compounds (9.20-9.94 eV) and cyclic carbonyl compounds (9.75-10.32 eV) from the decomposition channels of AnHP and KHP, respectively, as shown in Fig. S3(f). To summarize, these observations indicate that the conformational effects of heterocycle ring result in a large carbon flux entering the alternative isomerization pathways of OOγQOOH and the further decomposition reactions leading to AnHP – these pathways constitute an additional chain-branching reaction sequence for THP, which is in accordance with the findings for cyclohexane and its alkylated derivatives [16-18].

Of particular significance is the potential for ring-opening radicals within THPR2 and THPR4 to undergo oxygen addition, yielding linear peroxy radicals. Subsequently, these peroxy radicals may undergo intramolecular hydrogen migration, culminating in the formation of THP15DK3Q and THP1N6K3O4Q () intermediates. The presence of these intermediates is inferred from the PIE spectra depicted in Fig. 3c.

In this work, we also consider potential pathways involving third oxygen addition, as evidenced by the observed fragmentation of ionized OFDHP (m/z=115, $C_5H_7O_3$) and KDHP (m/z=131, $C_5H_7O_4$) species. The calculated APEs of $C_5H_7O_3$ and $C_5H_7O_4$, derived from the proposed representative structures, are 9.26-9.96 eV and 9.93-10.03 eV, respectively, which are consistent with the measured onset of the PIE spectra at 9.3 eV of m/z=115 and 9.9 eV of m/z=131 in Figs. S4(a) and Fig. S4(b), respectively. Similar to that of KHPs ($C_5H_8O_4$), Figure S5(a, b) illustrates that the temperature-dependent signal of $C_5H_7O_3$ and $C_5H_7O_4$ presents a hydroperoxide shape, which substantiates the similar chemical structure of these species. Furthermore, the calculated IEs of olefinic keto-hydroperoxides isomers (OFKHP, m/z=130, $C_5H_6O_4$) originating from olefinic dihydroperoxides (OFDHP, $C_5H_8O_5$), are presented in Fig. 3(d). Experimental onsets for m/z=130 align with the lower boundaries of calculated IEs. Despite challenges in detecting KDHP and OFDHP directly, the observed ionization fragments and temperature-dependent profiles as well as the potential dissociation products reinforce the occurrence of third oxygen addition. However, for simplification purpose, those third oxygen addition pathways are not considered in the present model.

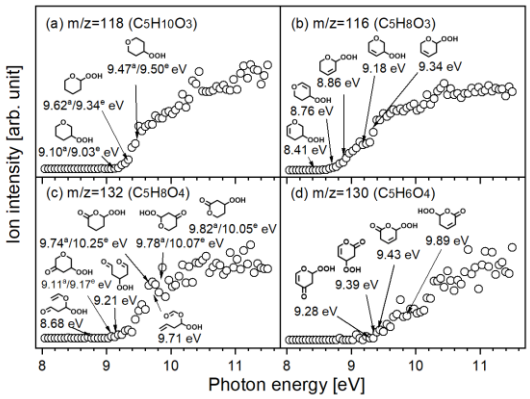

Fig. 3. PIE spectra of m/z=(a) 118, (b) 116, (c) 132, (d) 130 for THP oxidation in NSRL-JSR at 575 K, along with the molecular structures and calculated IEs of candidate isomers.

4.2 Measured and predicted species profiles

JSR experiments conducted in this study focus primarily on low- to intermediate-temperature chemistry, spanning the temperature range of 450-900 K, as illustrated in Fig. 4. The measured and predicted species profiles versus temperature reveal comprehensive insights into the oxidation process. Figure 4(a) shows that THP exhibits a notable negative temperature coefficient (NTC) behavior from lean to stoichiometric conditions, a characteristic well captured by the present model.

All simulations were performed using ANSYS Chemkin. Chemical mechanism and thermodynamic data files are available as *SM*.

The model performs quite reasonably in reproducing stable product profiles in lean mixtures, including O_2, H_2O, CO, CH_2O, CH_3OH, HOCHO, CH_3CHO, C_2H_4, with a maximum discrepancy of less than a factor of two, as shown in Fig. 3 and Fig. S8 (*SM*). Minor olefins like C_3H_6 and C_4H_6 are not as well predicted by the model. Additionally, the current model over-predicts the low-T reactivity at stoichiometric condition, showing areas for improvement. Total mole fractions of conjugated olefin and cyclic ether/ketone isomers are presented in Figs. 4(k,l) due to the experimental limitations of SVUV-PIMS in distinguishing these isomers. GC-MS facilitated the separation of isomers, and Figs. S9(a-d) in *SM* provide a detailed view of these profiles. The model successfully captured the formation of two conjugated olefins, 3,4-dihydro-2H-pyran and 3,6-dihydro-2H-pyran, as well as the production of cyclic ethers and glutaraldehyde.

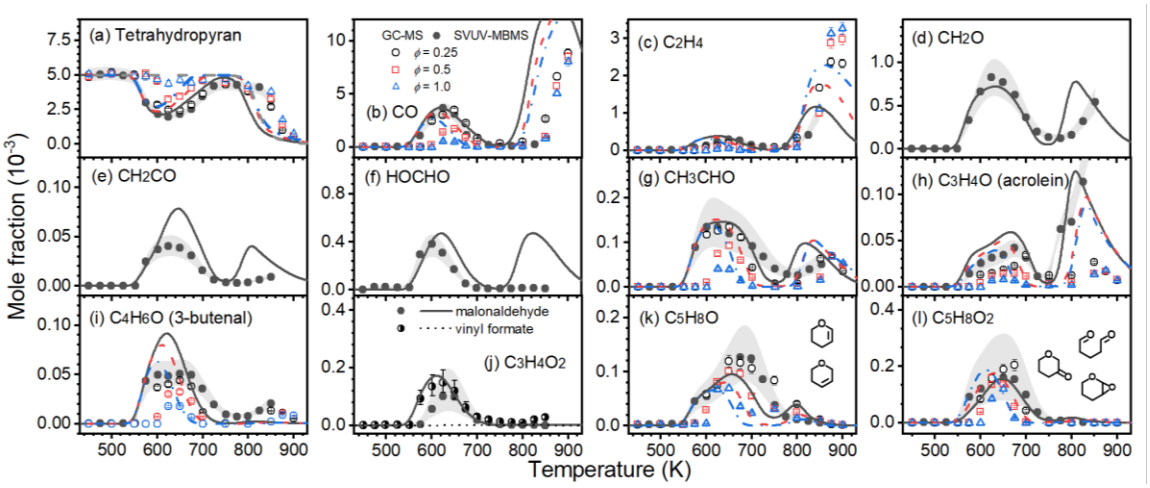

Fig. 4. Measured (symbols) and predicted (lines) results for tetrahydropyran (THP) oxidation in NSRL-JSR (~780 Torr) and *LRGP-JSR* (~800 Torr) at 0.5% THP, ϕ = 0.25 (○, circle), 0.5 (□, square), 1.0 (Δ, triangle) and τ = 4s. Gray dash line in (a) denote the simulated results using THP high-T oxidation and pyrolysis model [4]. The shaded region indicates the uncertainty of NSRL-JSR experiments.

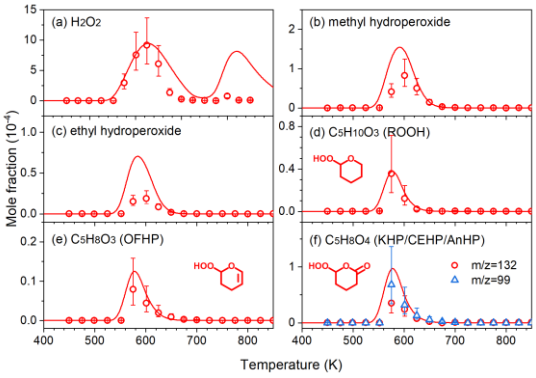

Fig. 5. Measured (symbols) and predicted (lines) hydroperoxides for THP oxidation in NSRL-JSR at 0.5% THP, ϕ = 0.25, and τ = 4s.

Validation against literature JSR high-T oxidation [5] and flow reactor pyrolysis [4] experiments demonstrates the reasonable performance of the model across a broader conditions. Those validations cover temperatures of 800-1133 K, pressures of 1-10 atm, and equivalence ratios of 0.5-2.0, as illustrated in Figs. S10 and S11 in *SM*. Interestingly, the current model and the Tran et al. [4] model both overpredict THP oxidation reactivity above 800 K, as shown in Fig.4(a), suggesting the need for further refinement of the intermediate- and high-T chemistry of THP.

The quantification of organic hydroperoxides is essential in elucidating low-temperature oxidation chemistry. Recently, Hu et al. [30] experimentally measured PICS for cyclohexyl hydroperoxide and 4-hydroperoxy-2-pentanone, enabling a quantitative assessment of organic hydroperoxides (i.e., ROOH, OFHP and KHP) in our investigation. In the case of KHP, both parent ions (m/z=132) and fragment ions (m/z=99, involving the loss of HO_2) were utilized for mole fraction determination, with uncertainties estimated within a factor of two. The results, as depicted in Fig. 5, demonstrate the model's adeptness in faithfully capturing the experimentally observed trends of hydroperoxides. In contrast to smaller hydroperoxides and stable oxidation products, $C_5H_8O_4$ (encompassing KHPs, AnHPs, and CEHPs) is formed at lower temperature of ~550 K and has a rapid decay (at ~620 K). This temporal pattern mirrors the initial decay phase of THP, as illustrated in Fig. 4(a), corroborating the pivotal role of KHP/AnHP in THP oxidation. Similar to KHP/AnHP, the observed temperature windows of $C_5H_{10}O_3$ (ROOH) and $C_5H_8O_3$ (OFHP) exhibit narrow spans, effectively captured by the current model.

Figure 4(e, f, i, j) further validates the predictive capability of the present model in reproducing the mole fractions of ketene, formic acid, 3-butenal, malonaldehyde and vinyl formate; these species result from hydroperoxide dissociation and heterocycle ring-opening pathways (*see Section 4.1*). These results underscore the model reliability in capturing the intricate carbon flux associated with various reaction pathways.

Rotavera et al. [7] and Davis et al. [8] employed MPIMS to discern the concerted elimination of peroxy radicals and the ring-opening reactions of R and QOOH radicals, respectively. Table S3 summarized the species detected and identified in the current work using SVUV-PIMS and GC-MS, alongside the literature findings [7, 8]. The abundance of identified species in the current study significantly contributes to our enhanced understanding of THP cool-flame chemistry.

4.3 Modeling analysis

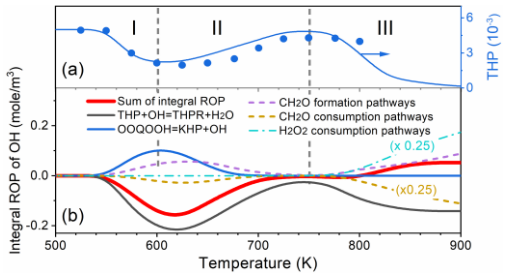

Fig. 6. (a) Mole fraction of THP; (b) Integrated ROP of OH. 0.5% THP, ϕ = 0.25, and τ = 4 s.

Consumption of THP and fuel radicals: To investigate the oxidation dynamics of THP and its impact on fuel radicals, we conducted a rate of production (ROP) analysis at $\phi = 0.25$ and $\tau = 4$ s, as shown in Fig. 7. Three temperatures, 575, 675, and 850 K, were selected to represent low-T (stage I: 550-625 K), NTC (stage II: 625-720 K), and high-T (stage III: 720-900 K) regions, as shown in Fig. 6(a). Figure S13(a) in *SM* synthesizes integrated ROP of THP at various temperatures, while Fig. S13(b) identifies the contributions of major pathways for THP consumption. It is seen that H-abstraction reactions by OH, HO_2, H, and O are important pathways contributing to THP consumption.

In stage I, H-abstraction by OH dominates THP consumption, contributing over 95% to fuel consumption at various temperatures, while contributions from HO_2 become increasingly important with rising temperature, reaching approximately 18% at 775 K. The presence of CH_2O at 650 K accentuates the contribution of H-abstraction by H radicals, amounting to 5% of THP consumption. This is mainly due to the abundance of CH_2O and carbonyl species formed in stage I, which enhance H generation via $CH_2O \rightarrow HCO \rightarrow H$ in stage II.

The existence of an ether group in THP contributes to three distinct C-H bond strengths at its *ortho*- (95.1 kcal/mol), *meta*- (99.2 kcal/mol), and *para*- (97.8 kcal/mol) sites [23], influencing the formation of fuel radicals through H-abstraction, and resulting in three fuel radicals (THPR2, THPR3, THPR4). ROP analysis in Fig. S7 indicates that 95% of R undergoes barrierless oxygen addition forming ROO at 575 K, and this ratio decreases to 62% at 675 K. Moreover, the ring-opening channel of fuel radical has a significant contribution for R consumption, which increases from 2% at 575 K to 37% at 675 K. Rotavera et al. [7] calculated β-dissociation energies of THPR2, THPR3, and THPR4 to be 3.7, 17.0, and 18.1 kcal/mol, respectively, indicating the significant contribution of ring-opening reactions for fuel radical consumption.

Chain branching process in low-T region: A simplified reaction network involving OH, H, and HO_2 radicals is illustrated in Fig. S12. The KHP channel (ROO↔γQOOH↔OOγQOOH→KHP→XO+OH) is responsible for OH formation in stage I of THP oxidation. Carbon flux analysis based on Fig. 7 indicates that both the conventional KHP channel and the additional AnHP channel (ROO↔γQOOH↔OOγQOOH→γ$(POOH)_2$→AnHP/4mCEHP →XO+OH) play a pivotal role in the chain-branching process. Remarkably, 42% and 19% of fuel carbon enters KHP channels and AnHP channels, respectively, at 575 K. This ratio diminishes to 7% and 4% at 675 K.

ROO radicals undergo intramolecular H-transfer forming γQOOH. This reaction is the third step in forming OOγQOOH, explaining its significance in the chain-branching process. THPROO2, THPROO3, and THPROO4 contribute to this process, with the extent of their participation influenced by the distinct reactivity of peroxy radicals due to the presence of the ether group in THP. THPROO3 can undergo a single 1,5-H shift channel, forming THP3Q5J (), with an energy barrier of 28.0 kcal/mol, whereas THPROO2 can undergo two effective channels via 1,5-H shift, forming THP2Q6J () and THP2Q4J (), with energy barriers of 20.4 kcal/mol and 25.3 kcal/mol, respectively. Moreover, THPROO4 can undergo two effective 1,5-H shift channels, forming THP4Q2J (), with an energy barrier of 23.9 kcal/mol. Figure 2 illustrated that the energy barrier in OOQOOHs show a similar trend as ROO. The difference in energy barriers is mainly due to the BDE of the abstracted C-H, as shown in Fig.1.

Therefore, similar to the THP molecule, the ether group of heterocycle ring in fuel-specific peroxy radicals can result in a stronger C-H bond at its *meta*-site and a weaker C-H at its *ortho*-site, ultimately changing the reactivity of the corresponding peroxy radicals. ROP analysis reveals that only 24% THPROO3 can undergo 1,5-H shift to form γQOOH (THP3Q5J) at 575 K, while these values are 87% and 91% for THPROO2 and THPROO4, respectively. On the contrary, 16% THPROO3 contributes to conjugated olefins formation, and the remaining 51% THPROO3 undergoes bimolecular reactions to end the chain-branching process. The constrained carbon flux identified in THP3Q5J has the capacity to generate only a limited amount of THP3K5Q through secondary reaction pathways. This finding implies that the observed ionization thresholds of the PIE spectra of m/z=132 is associated with the formation of THP15DK3Q originating from the AnHP channel. In summary, the carbon flux entering THPR3 leads to chain-inhibition, while the carbon flux entering THPR2 and THPR4 contributes to chain-branching in stage I and stage II. Thus, fuel consumption and product formation are sensitive to the branching ratio of H-abstraction of THP by OH. However, only a limited number of experimental results reported the total rates of OH+THP [24, 31] at 263-372 K, and no data are available under combustion-relevant conditions; this is a major source of uncertainty in the modeling performance illustrated in Section 4.2.

Additionally, CH_2CHO radical, resulting from the unimolecular decomposition of oxy radicals (XOs) can contribute to approximately 20% OH formation at 575K via $CH_2CHO+O_2 \rightarrow CH_2O+CO+OH$ and $CH_2CHO+O_2 \rightarrow O_2CH_2CHO \rightarrow HO_2CH_2CO \rightarrow CH_2O+CO+OH$. This contribution increases to 56% at 650 K, as shown in Fig. 6(b). On the other hand, the consumption of CH_2O can contribute to 9% for OH consumption, and this contribution increases to 20% at 650 K.

Chemistry in NTC and high-T regions: With increasing temperature, the low-T chain-branching process is inhibited. The enhanced reverse reactions of oxygen addition, the increased contributions of reactions leading to less reactive species (HO_2, olefins, cyclic ethers), and the heightened unimolecular decomposition of fuel radicals and QOOHs contribute to the NTC behavior observed in stage II. As a result, the carbon flux in KHP/AnHP channels decreases from 61% at 575 K to 11% at 675 K, while the carbon flux of the fuel radical ring-opening channel increases from 4% at 575 K to 35% at 675 K. Meanwhile, the carbon flux of HO_2-concerted elimination channels increases from 6% at 575 K to 11% at 675 K. This shift of carbon-flux between chain-inhibition and chain-branching channels ultimately leads to the fact that the contribution of the KHP channel to OH formation decrease from 66% at 575 K to 12% at 675K. Consequently, an apparent NTC behavior is observed in THP oxidation, as shown in Fig.6(b).

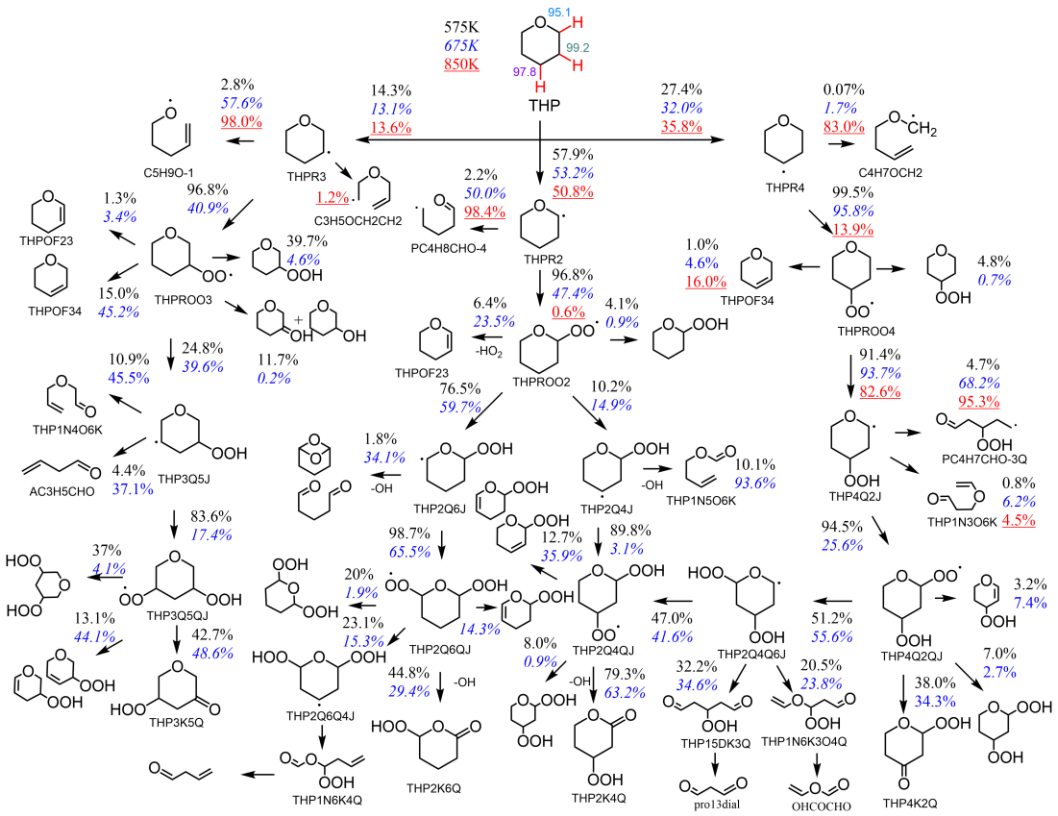

Fig.7 ROP analysis in low-T oxidation of THP at ϕ = 0.25, τ = 4 s, 1.04 bar and temperatures of 575 K (black percentages), 675 K (blue italic percentages) and 850 K (red underlined percentages).

In stage III, OH formation is promoted via $H_2O_2(+M)=2OH(+M)$ and two additional minor channels: $H_2O_2+H=H_2O+OH$ and $ally+HO_2=C_3H_5O+OH$, resulting in the sum of ROP integral of OH changing from negative to positive. Moreover, Fig. 7 indicates that 92% of fuel radicals undergo unimolecular decomposition by ring-rupture forming acyclic isomers underscoring the significance of ring-opening reactions in stage III. Besides, H-atoms from CH_2O chemistry and O-atoms from $O_2+H=O+OH$ and $C_2H_3+O_2=CH_2CHO+O$ significantly enrich the radical pool in stage III. Consequently, fuel consumption is significantly enhanced in the high-T region, as shown in Fig.S13(b).

5. Conclusions

This study presents the first-ever experimental investigation of THP oxidation in two JSRs, covering the temperature range of 450-900 K, specifically focusing on the low- to intermediate-temperature regime. A variety of intermediates, including olefins, C_1-C_4 carbonyl compounds, conjugated olefins, cyclic ethers, and hydroperoxides, were qualitatively and quantitatively analyzed using SVUV-PIMS and GC-MS diagnostic methods supported by theoretical quantum calculations. To simulate the observed species data from both the current JSR experiments and literature data, a comprehensive kinetic model of THP oxidation was developed. This model considers the conformational effects of the heterocycle ring, incorporating separated *cis*-OOγQOOH and *trans*-OOγQOOH conformers. This model was further validated by identifying alkenal-hydroperoxides (AnHP) and their decomposition products. Comparison with cyclohexane revealed that the ether group in the heterocycle ring of ROO and OOQOOH radicals influences the C-H BDE, strengthening the bond at the *meta*-site while weakening it at the *ortho*-site. In the low-T region, the ether group's influence promotes chain-inhibition for reactions originating from β-tetrahydropyranyl, while chain-branching reactions become more favorable for reactions stemming from α-and γ-tetrahydropyranyl. As temperature increases, α- and β-tetrahydropyranyl radicals tend to undergo ring-opening, and the reverse reaction of oxygen addition and concerted elimination reactions of peroxy radicals become more significant. This leads to a pronounced NTC behavior in THP oxidation. The results of this work aid in an improved understanding of low-*T* oxidation molecules with a heterocycle ring.

Acknowledgments

This work was funded by the Office of Sponsored Research (OSR) at King Abdullah University of Science and Technology (Grant URF/1/435101-01 CRG 2020), National Natural Science Foundation of China (51976028) and Key Collaborative Research Program of

the Alliance of International Science Organization (grant no. ANSO-CR-KP-2022-04).

Supplementary material

Additional materials, measured JSR data, and CHEMKIN-compatible mechanism files are provided.

References

[1] L.D. Schmidt, P.J. Dauenhauer, Hybrid routes to biofuels, Nature 447 (2007) 914-915.
[2] B. Rotavera, C.A. Taatjes, Influence of functional groups on low-temperature combustion chemistry of biofuels, Prog. Energy Combust. Sci. 86 (2021) 100925.
[3] L.-S. Tran, O. Herbinet, H.-H. Carstensen, F. Battin-Leclerc, Chemical kinetics of cyclic ethers in combustion, Prog. Energy Combust. Sci. 92 (2022) 101019.
[4] L.-S. Tran, R. De Bruycker, H.-H. Carstensen, P.-A. Glaude, F. Monge, M.U. Alzueta, R.C. Martin, F. Battin-Leclerc, K.M. Van Geem, G.B. Marin, Pyrolysis and combustion chemistry of tetrahydropyran: Experimental and modeling study, Combust. Flame 162 (2015) 4283-4303.
[5] P. Dagaut, M. McGuinness, J. Simmie, M. Cathonnet, The ignition and oxidation of tetrahydrofuran: Experiments and kinetic modeling, Combust. Sci. Tech. 135 (1998) 3-29.
[6] N.J. Labbe, V. Seshadri, T. Kasper, N. Hansen, P. Oßwald, P.R. Westmoreland, Flame chemistry of tetrahydropyran as a model heteroatomic biofuel, Proc. Combust. Inst. 34 (2013) 259-267.
[7] B. Rotavera, J.D. Savee, I.O. Antonov, R.L. Caravan, L. Sheps, D.L. Osborn, J. Zádor, C.A. Taatjes, Influence of oxygenation in cyclic hydrocarbons on chain-termination reactions from R+O_2: Tetrahydropyran and cyclohexane, Proc. Combust. Inst. 36 (2017) 597-606.
[8] J.C. Davis, A.L. Koritzke, R.L. Caravan, I.O. Antonov, M.G. Christianson, A.C. Doner, D.L. Osborn, L. Sheps, C.A. Taatjes, B. Rotavera, Influence of the ether functional group on ketohydroperoxide formation in cyclic hydrocarbons: Tetrahydropyran and cyclohexane, J. Phys. Chem. A 123 (2019) 3634-3646.
[9] M.-W. Chen, B. Rotavera, W. Chao, J. Zádor, C.A. Taatjes, Direct measurement of ˙OH and HO_2˙ formation in ˙R+O_2 reactions of cyclohexane and tetrahydropyran, Phys. Chem. Chem. Phys. 20 (2018) 10815-10825.
[10] H. Telfah, M.A. Reza, J. Alam, A.C. Paul, J. Liu, Direct observation of tetrahydrofuranyl and tetrahydropyranyl peroxy radicals via cavity ring-down spectroscopy, J. Phys. Chem. Lett. 9 (2018) 4475-4480.
[11] Q. Xu, B. Liu, W. Chen, T. Yu, Z. Zhang, C. Zhang, L. Wei, Z. Wang, Comprehensive study of the low-temperature oxidation chemistry by synchrotron photoionization mass spectrometry and gas chromatography, Combust. Flame 236 (2022) 111797.
[12] T.A. Cool, K. Nakajima, C.A. Taatjes, A. McIlroy, P.R. Westmoreland, M.E. Law, A. Morel, Studies of a fuel-rich propane flame with photoionization mass spectrometry, Proc. Combust. Inst. 30 (2005) 1681-1688.
[13] I. Meziane, N. Delort, O. Herbinet, R. Bounaceur, F. Battin-Leclerc, A comparative study of the oxidation of toluene and the three isomers of xylene, Combust. Flame 257 (2023) 113046.
[14] A.D. Becke, Density-functional thermochemistry. III. The role of exact exchange, J. Chem. Phys. 98 (1993) 5648-5652.
[15] M.J. Frisch, et al., Gaussian 09, Gaussian, Inc., Wallingford CT, 2013.
[16] J.B. Zou, H.F. Jin, D.P. Liu, X.Y. Zhang, H.J. Su, J.Z. Yang, A. Farooq, Y.Y. Li, A comprehensive study on low-temperature oxidation chemistry of cyclohexane. II. Experimental and kinetic modeling investigation, Combust. Flame 233 (2021) 111550.
[17] J.B. Zou, J.G. Zhang, T.Y. Lian, Q. Xu, B.Z. Liu, Z.D. Wang, J.Z. Yang, Y.Y. Li, Conformation-dependent low-temperature oxidation chemistry of methylcyclohexane: First oxygen addition and chain-branching, Combustion and Flame 243 (2022).
[18] J.B. Zou, Y.Y. Li, L.L. Ye, H.F. Jin, A comprehensive study on low-temperature oxidation chemistry of cyclohexane. I. Conformational analysis and theoretical study of first and second oxygen addition, Combust. Flame 233 (2021) 111658.
[19] S.M. Burke, W. Metcalfe, O. Herbinet, F. Battin-Leclerc, F.M. Haas, J. Santner, F.L. Dryer, H.J. Curran, An experimental and modeling study of propene oxidation. Part 1: Speciation measurements in jet-stirred and flow reactors, Combust. Flame 161 (2014) 2765-2784.
[20] S.W. Benson, Thermochemical kinetics, Wiley1976.
[21] M. Verdicchio, B. Sirjean, L.S. Tran, P.-A. Glaude, F. Battin-Leclerc, Unimolecular decomposition of tetrahydrofuran: Carbene vs. diradical pathways, Proc. Combust. Inst. 35 (2015) 533-541.
[22] Y.R. Luo, Comprehensive handbook of chemical bond energies, CRC press2007.
[23] C. Huang, Y. Zhao, I.S. Roy, L. Cai, H. Pitsch, K. Leonhard, Effect of methyl substituents, ring size, and oxygen on bond dissociation energies and ring-opening kinetics of five- and six-membered cyclic acetals, Combust. Flame 242 (2022) 112211.
[24] J. Moriarty, H. Sidebottom, J. Wenger, A. Mellouki, G. Le Bras, Kinetic studies on the reactions of hydroxyl radicals with cyclic ethers and aliphatic diethers, J. Phys. Chem. A 107 (2003) 1499-1505.
[25] V. Saheb, A. Bahadori, Theoretical studies on the kinetics of the hydrogen-abstraction reactions from 1, 3, 5-trioxane and 1, 4-dioxane by OH radicals, Prog. React. Kinet. Mech. 45 (2020) 1-13.
[26] M. Hellmuth, B. Chen, C. Bariki, L. Cai, F. Cameron, A. Wildenberg, C. Huang, S. Faller, Y. Ren, J. Beeckmann, K. Leonhard, K.A. Heufer, N. Hansen, H. Pitsch, A comparative study on the combustion chemistry of two bio-hybrid fuels: 1,3-dioxane and 1,3-dioxolane, J. Phys. Chem. A 127 (2022) 286-299.
[27] S. Handford-Styring, R. Walker, Arrhenius parameters for the reaction HO_2 + cyclohexane between 673 and 773 K, and for H atom transfer in cyclohexylperoxy radicals, Phys. Chem. Chem. Phys. 3 (2001) 2043-2052.
[28] C. Huang, Y. Zhao, I.S. Roy, B. Chen, N. Hansen, H. Pitsch, K. Leonhard, Pathway exploration in low-temperature oxidation of a new-generation bio-hybrid fuel 1,3-dioxane, Proc. Combust. Inst. 39 (2022) 385-393.
[29] C.F. Goldsmith, W.H. Green, S.J. Klippenstein, Role of O_2 + QOOH in low-temperature ignition of propane. 1. Temperature and pressure dependent rate coefficients, J. Phys. Chem. A 116 (2012) 3325-3346.
[30] Z. Hu, Q. Di, B. Liu, Y. Li, Y. He, Q. Zhu, Q. Xu, P. Dagaut, N. Hansen, S.M. Sarathy, L. Xing, D.G. Truhlar, Z. Wang, Elucidating the photodissociation fingerprint and quantifying the determination of organic hydroperoxides in gas-phase autoxidation, Proc. Natl. Acad. Sci. U. S. A. 120 (2023) e2220131120.
[31] P. Dagaut, R. Liu, T.J. Wallington, M.J. Kurylo, Flash photolysis resonance fluorescence investigation of the gas-phase reactions of hydroxyl radicals with cyclic ethers, J. Chem. Phys. 94 (1990) 1881-1883.